NANO LETTERS

Letter

pubs.acs.org/NanoLett

Competing Gap Opening Mechanisms of Monolayer Graphene and Graphene Nanoribbons on Strong Topological Insulators

Zhuonan Lin,[†,‡] Wei Qin,[‡] Jiang Zeng,[‡,§] Wei Chen,[‡,∥] Ping Cui,[‡] Jun-Hyung Cho,[‡,⊥] Zhenhua Qiao,[‡,#] and Zhenyu Zhang*[,‡]

[†]School of Physics and Technology, Wuhan University, Wuhan 430072, China

[‡]International Center for Quantum Design of Functional Materials (ICQD), Hefei National Laboratory for Physical Sciences at the Microscale, and Synergetic Innovation Center of Quantum Information and Quantum Physics, University of Science and Technology of China, Hefei, Anhui 230026, China

[§]Beijing Computational Science Research Center, Beijing 100094, China

[∥]Department of Physics and School of Engineering and Applied Sciences, Harvard University, Cambridge, Massachusetts 02138, United States

[⊥]Research Institute for Natural Sciences, Hanyang University, Seoul 133-791, Korea

[#]CAS Key Laboratory of Strongly-Coupled Quantum Matter Physics and Department of Physics, University of Science and Technology of China, Hefei, Anhui 230026, China

S *Supporting Information*

ABSTRACT: Graphene is a promising material for designing next-generation electronic and valleytronic devices, which often demand the opening of a bandgap in the otherwise gapless pristine graphene. To date, several conceptually different mechanisms have been extensively exploited to induce bandgaps in graphene, including spin−orbit coupling and inversion symmetry breaking for monolayer graphene, and quantum confinement for graphene nanoribbons (GNRs). Here, we present a multiscale study of the competing gap opening mechanisms in a graphene overlayer and GNRs proximity-coupled to topological insulators (TIs). We obtain sizable graphene bandgaps even without inversion symmetry breaking and identify the Kekulé lattice distortions caused by the TI substrates to be the dominant gap opening mechanism. Furthermore, Kekulé distorted armchair GNRs display intriguing non-monotonous gap dependence on the nanoribbon width, resulting from the coexistence of quantum confinement, edge passivation, and Kekulé distortions. The present study offers viable new approaches for tunable bandgap engineering in graphene and GNRs.

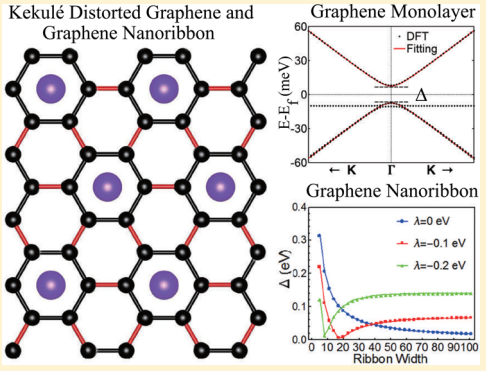

KEYWORDS: *First-principles calculations, graphene, graphene nanoribbons, Kekulé distortions, gap opening*

Graphene is a representative two-dimensional (2D) material consisting of a monolayer of carbon atoms arranged on a honeycomb lattice. The unique sublattice symmetry of such a 2D hexagonal system leads to a particular gapless Dirac cone structure at the corners of the corresponding Brillouin zone (BZ).[1] Associated with its novel electronic properties, graphene has been exploited as an ideal platform for observation of many intriguing phenomena, such as Klein tunneling,[2] ballistic transport,[3] and different types of Hall effects.[4−10] Many of these pioneering studies invoked the opening of a band gap in graphene, which leads to the emergence of a variety of topologically nontrivial states. Once realized, such exotic quantum states in graphene may have important applications in spintronics and valleytronics.

Several conceptually different mechanisms have been exploited to open a band gap in graphene. The first is to use diluted heavy adatoms or proper substrates to enhance the spin−orbit coupling (SOC), which in turn can open a gap in graphene.[11−14] The second relies on the breaking of the sublattice symmetry on a substrate of proper symmetry such as SiC or h-BN.[15−18] The third is to induce inequivalent hopping rates between the sublattice sites, leading to intervalley scattering of the Dirac electrons,[19] for example, via Kekulé distortions in the graphene lattice.[20−22] Finally, for graphene in reduced geometry such as graphene nanoribbons (GNRs), quantum size effects can result in tunable band gaps as a function of the ribbon width.[23−29]

Here, we present a systematic study of the electronic properties of monolayer graphene and graphene nanoribbons on three-dimensional (3D) topological insulators (TIs), which, strikingly, allow us to explore the delicate competitions of most

Received: December 26, 2016
Revised: May 19, 2017
Published: May 23, 2017

ACS Publications © XXXX American Chemical Society

DOI: 10.1021/acs.nanolett.6b05354
Nano Lett. XXXX, XXX, XXX−XXX

of the gap opening mechanisms outlined above. We first use first-principles calculations to reveal that a graphene overlayer exhibits stronger proximity-induced Rashba SOC splits and a larger band gap in its band structure on Sb_2Te_3 than on Bi_2Te_3, even though the latter TI inherently possesses stronger SOC. The underlying reason is attributed to the smaller lattice mismatch between graphene and Sb_2Te_3, leading to a closer graphene/TI interface spacing and correspondingly stronger Kekulé distortions on the graphene honeycomb lattice. We also identify that the opened gaps of about 18 and 5 meV for graphene on Sb_2Te_3 and Bi_2Te_3 are primarily due to the Kekulé lattice distortions caused by the TI substrates, rather than the prevailing belief of proximity-enhanced SOC effects.[30,31] The 5 meV gap for the latter system is an upper limit, for reasons to be elaborated later. Next, we develop a generic tight-binding (TB) description to investigate the competing gap opening mechanisms of such Kekulé distorted graphene monolayer and graphene nanoribbons (KGNRs). For Kekulé distorted graphene, the band gap scales linearly with the strength of the distortion. In contrast, the band gaps of armchair KGNRs may display intriguing nonmonotonous scaling behaviors with respect to the ribbon width, resulting from the coexistence of quantum confinement, edge passivation, and Kekulé distortions. The present study helps to clarify on some existing misperceptions surrounding gap opening mechanisms of graphene on TI substrates, and the central results effectively enrich possible approaches toward inducing tunable band gaps in graphene and graphene nanoribbons.

First-principles calculations within DFT were performed using the Vienna *ab initio* simulation package.[33,34] The generalized gradient approximation of Perdew–Burke–Ernzerhof type functional was employed to treat the exchange-correlation potential of electrons.[35] Projected augmented wave potentials were employed to represent the ions. The spin–orbit coupling effects were treated by using scalar-relativistic eigenfunctions as the basis set, and van der Waals interactions were included using the DFT-D3 method.[36] A cutoff energy of 500 eV was used to expand the wave functions and potentials in the plane-wave basis. An 11 × 11 × 1 Monkhorst mesh was used in *k*-space to sample the Brillouin zone,[37] and a 15 Å thick vacuum layer was introduced to avoid possible effects between image supercells.

The heterostructures consisting of a graphene monolayer on the (111) surface of Sb_2Te_3 or Bi_2Te_3 are shown in in Figure 1a. Here, we model the TIs with three quintuple layers (QLs) to avoid significant interactions between the two types of topological surface states.[38,39] As shown in Table 1, the in-plane lattice constant of Sb_2Te_3 is about 4.25 Å, giving a lattice mismatch of about 0.47% between the substrate and a perfectly commensurate $\sqrt{3} \times \sqrt{3}$ graphene superlattice. The superlattice constant is about 4.27 Å, while the carbon–carbon bond length is 1.422 Å.[28] Given the extremely small lattice mismatch, it is natural to expect that in the graphene/Sb_2Te_3 heterostructure, the carbon atoms will be compressed to follow the periodicity of the TI substrate,[30] mimicking the physically realistic situation of a sufficiently large graphene overlayer on the TI. Furthermore, we focus on a physically realistic case where the crystallographic axes of graphene and Sb_2Te_3 are perfectly aligned. For the graphene/Bi_2Te_3 system, the lattice mismatch of ∼2.58% is too large for the overlayer to grow epitaxially with mutually matching lattices,[40,41] but for comparison purposes and realistic computational concerns we stretch the graphene lattice to also match that of the TI substrate. In doing so, the graphene–TI coupling is somewhat overestimated, irrespective of the nature of the coupling (e.g., SOC or Kekulé); therefore, the opened gap can only be viewed as an upper limit.

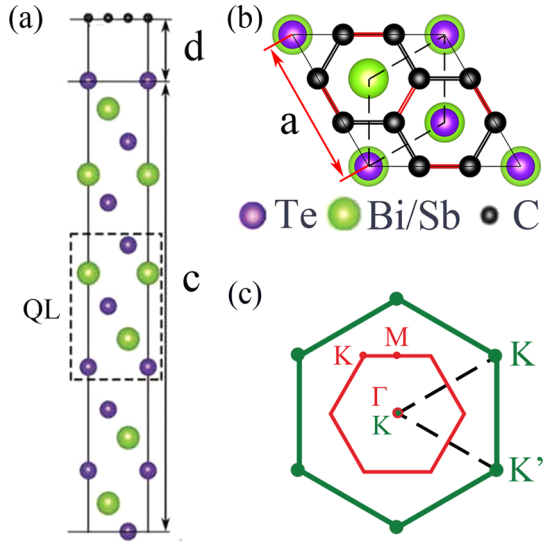

Figure 1. Lattice structures of graphene/TI heterostructures. (a,b) Illustrations of the graphene/TI heterostructures from (a) the side view and (b) the top view. In (b), the dashed rhombus indicates the 1 × 1 unit cell of pristine graphene, while the larger rhombus encompassing the systems indicates the $\sqrt{3} \times \sqrt{3}$ unit cell of the graphene/TI heterostructures. (c) BZ of pristine graphene (green) and folded BZ of Kekulé graphene as distorted by the TI substrates (red).

Table 1. Structural Parameters of the Graphene/TI Heterostructures[a]

TI	*a* (Å)	*c* (Å)	*d* (Å)	mismatch (%)	|λ| (meV)
Bi_2Te_3	4.38	30.49	3.87	2.58	2.5
Sb_2Te_3	4.25	30.35	3.59	0.47	8.0

[a]Lattice constants *a* and *c* of the TIs were taken from ref 47. The interfacial distances *d* between graphene and the TI substrates were calculated through structurally optimization. The strengths of the Kekulé distortions |λ| are extracted by fitting the first-principle data within the tight-binding model described by eq 2.

With the hexagonal nature of the in-plane lattice structures of the TI substrates, the interaction between the graphene overlayer and the TIs leads to Kekulé distortions in the honeycomb lattice of graphene as illustrated in Figure 1b. The equilibrium interfacial distances between the graphene overlayer and the TI substrates listed in Table 1 are calculated with the inclusion of the van der Waals-type interaction. By comparing the results for the two types of TI substrates, we find that a smaller lattice mismatch results in a closer interfacial coupling and potentially stronger Kekulé distortions.

Figure 2 shows the band structures of the graphene/TI heterostructures obtained by the density functional theory (DFT) calculations with the Fermi level set to be zero. For both systems, the graphene bands near the Γ-point display Rashba-type splits, arising from the proximity coupling between the graphene and substrates.[42] As shown in Figure 2c,d, the Rashba splitting around the Γ-point is much larger on Sb_2Te_3 than on Bi_2Te_3. More significantly, a sizable overall band gap of ∼18 meV is present for the graphene/Sb_2Te_3 system, while the much smaller band gap of ∼5 meV for graphene on Bi_2Te_3 still

DOI: 10.1021/acs.nanolett.6b05354
Nano Lett. XXXX, XXX, XXX–XXX

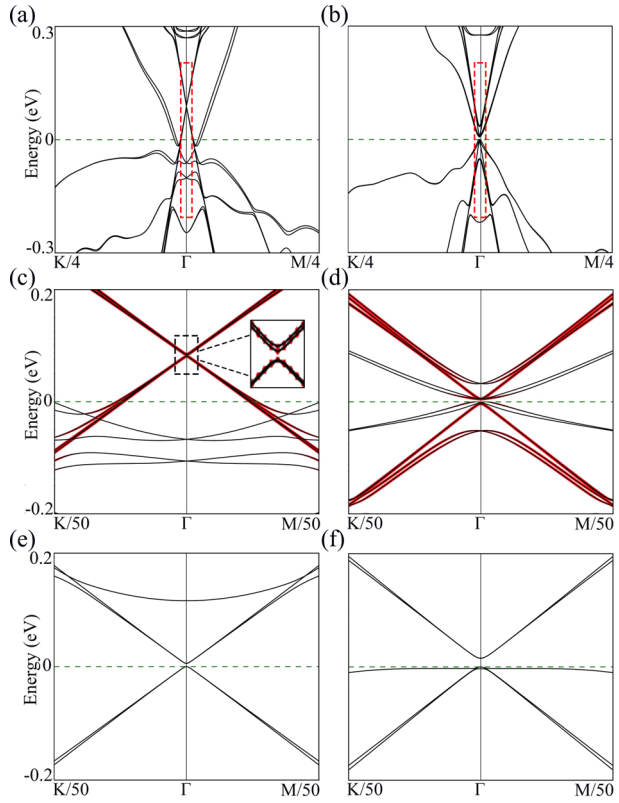

Figure 2. Band structures of graphene/Bi_2Te_3 (left panels) and graphene/Sb_2Te_3 (right panels). The zoomed-in portions in (a,b) are given in (c,d), respectively. The states marked in red represent the contributions from the carbon atoms. (e,f) The corresponding band structures of the two types of graphene/TI heterostructures, obtained without SOC.

serves as an upper limit as a result of the artificially matched lattices, which, as noted earlier, could overestimate the Kekulé distortions. Qualitatively, the stronger Rashba SOC splits and the larger gap in the band structure of graphene/Sb_2Te_3 can both be attributed to the closer interfacial coupling in this system.

As for the dominant gap opening mechanism in these heterostructures, it is tempting to identify the proximity-enhanced SOC effects in graphene to be responsible, as proposed recently in closely related studies of graphene/TI systems.[30,31] However, our closer analysis of the SOC effects clearly rules out this possibility. As shown in Figure 2e,f, we find comparable energy gaps in the two types of heterostructures when the spin−orbit interactions are completely suppressed, given by ∼16 and ∼5 meV, respectively. On the outer side, from Figure 1b, we note that the on-site energies of carbon atoms at the two sublattice sites remain degenerate when graphene overlayer is on either of the two types of TI substrates; therefore, the gap opening can not be attributed to breaking of the sublattice symmetry either. Furthermore, the potential effect of electron−phonon coupling is absent in the present study and is therefore unable to account the gap opening as observed.[32]

On the basis of the above analyses, the only remaining likely gap opening mechanism in these systems is due to the Kekulé distortions of the gaphene lattice by the TI substrates. A Kekulé distorted graphene is characterized by two types of inequivalent hopping rates between the carbon atoms. As illustrated in Figure 1b, such hopping differences stem from the presence or absence of an additional hopping channel between two neighboring carbon atoms, mediated by the availability of a topmost Te atom layer. Qualitatively, the mechanism of Kekulé distortion-induced band gap opening in graphene can be well understood from Figure 1c, where the $\sqrt{3} \times \sqrt{3}$ superlattice folds K and K′ valleys of pristine graphene unit cell to the Γ-point in the heterostructure and the Kekulé distortion couples the two valleys, lifting the degeneracy, thus giving rise to the band gaps as obtained from the detailed computational studies.[19]

To gain more insights into the underlying physics involved and also reveal the generic trends in such systems, we develop a TB model to describe the Kekulé distorted graphene in connection with the DFT results, which enable us to quantitatively extract the strengths of the Kekulé distortions. This approach also allows us to readily explore the novel electronic and transport properties of KGNRs. The distorted lattice structure is shown in Figure 3a, where every independent

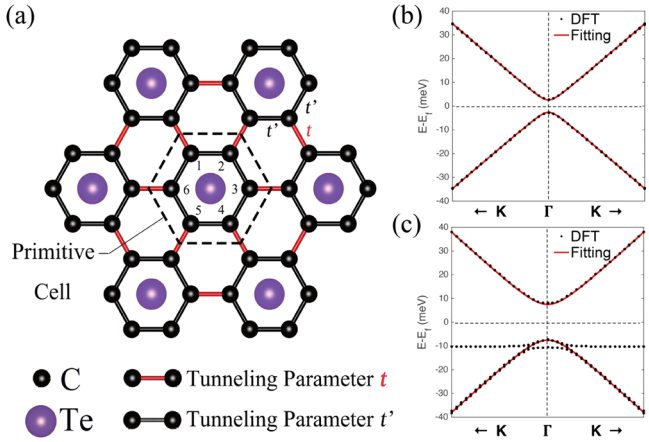

Figure 3. (a) Schematic of Kekulé distorted graphene lattice. (b,c) Band structures of graphene on (b) Bi_2Te_3 and (c) Sb_2Te_3 with the dots representing the first-principles data calculated without SOC and lines (red) the TB fittings.

hexagonal carbon circle of graphene encompasses a Te atom, which dominates the contribution to the Kekulé distortions, giving rise to two different hopping rates. The Kekulé distorted graphene can be described by the Hamiltonian

$$H_0 = t \sum_{i=1}^{3} (a_i^\dagger a_{i+3} + \text{H.c.}) + t' \sum_{i=1}^{6} (a_i^\dagger a_j + \text{H.c.}) \quad (1)$$

where t = 2.7 eV is the nearest-neighbor hopping energy of pristine graphene,[43] t' is an effective hopping energy modified by the substrates, $a_i^\dagger$ is the Fermionic creation operator acting on site i, and $j = i + 1$ is the next site of i along the clockwise direction shown in Figure 3a, with the periodic boundary constraint of period 6. For the special case $t = t'$, Hamiltonian (1) restores the TB description of pristine graphene. By expanding the operator in the momentum space as $a_i = \frac{1}{\sqrt{N_0}} \sum_{\mathbf{k}} a_{i,k} \exp(i\mathbf{k}\cdot\mathbf{R}_i)$, where N_0 is the normalization parameter, $\boldsymbol{k}$ runs over the first BZ, we obtain the band structure of the Kekulé distorted graphene with a opened gap at the Γ-point. By performing block diagonalization around the BZ center, we further extract a 4 × 4 low-energy effective Hamiltonian as

DOI: 10.1021/acs.nanolett.6b05354
Nano Lett. XXXX, XXX, XXX−XXX

$$H_{\text{eff}} = \nu_F(k_x\sigma_x\tau_z + k_y\sigma_y) + \lambda\sigma_x\tau_x \quad (2)$$

where $\nu_F = 3ta/2$ is the Fermi velocity, a is the carbon−carbon distance, $\sigma_{x,y}$ and $\tau_{x,z}$ are the Pauli matrices acting on the real-space sublattices and momentum-space valleys, respectively, and $\lambda = t - t' < 0$ measures the strength of the Kekulé distortions. The corresponding energy spectra are given by $\epsilon_{\pm}(k) = \pm\sqrt{\nu_F^2|\mathbf{k}|^2 + \lambda^2}$, indicating the emergence of a massive single-particle energy gap due to the intervalley scattering. Equation 2 also shows that the gap size scales linearly with the strength of the Kekulé distortions. Furthermore, as shown in Figure 3b,c, by fitting the band structures of Kekulé distorted graphene shown in Figure 2e,f within the low-energy effective model described by eq 2, we find the strength of Kekulé distortions in graphene on Bi_2Te_3 and Sb_2Te_3 to be $\lambda \sim -2.5$ and -8 meV, respectively.

Next we shift our attention to the KGNRs. As references, earlier studies have shown that GNRs with different types of edges exhibit different electronic properties.[23−28] For zigzag GNRs, there always exist metallic edge states on both sides of the ribbon,[45] unless the antiferromagnetic coupling between the edge states is considered, which transforms the system into a nonconducting state when the ribbon width is narrow enough.[44] However, for armchair GNRs the band gaps scale monotonously with the widths as a consequence of the quantum confinement and edge passivation.[28,29] Here, our detailed studies without considering spin polarization show that the electronic properties of the zigzag KGNRs still possess gapless edges states. In contrast, the electronic properties of armchair KGNRs display rich features as a result of different competing gap opening mechanisms, as detailed below.

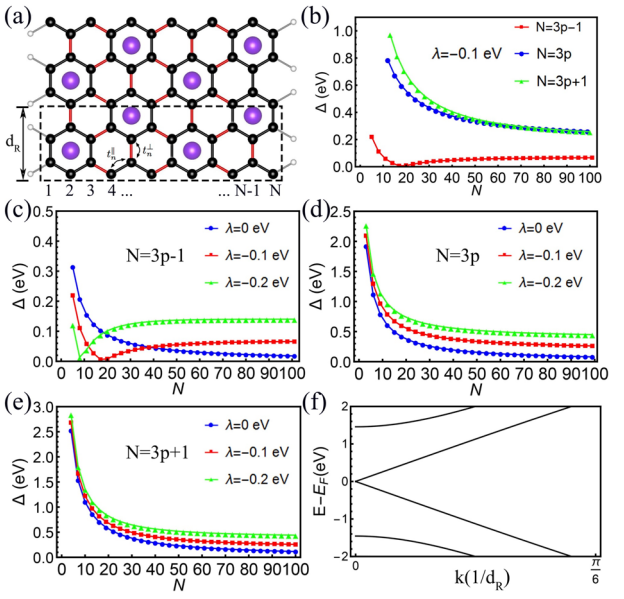

Figure 4. Band gaps of armchair KGNRs (a) Schematic of an armchair KGNR with width $N = 12$, whose edge atoms are passivated by hydrogen atoms. (b) Band gap variations as functions of the ribbon width with $\lambda = -0.1$ eV. (c−e) Band gap variations as functions of the width and distortion strength for (c) $N = 3p-1$, (d) $N = 3p$, and (e) $N = 3p + 1$. (f) Band structure of a specific system with $\lambda = -0.2$ eV and $N = 8$.

As shown in Figure 4a, the armchair KGNRs are classified by the number of dimer bonds N across the ribbon width. The corresponding TB Hamiltonian is given as

$$H_r = \sum_{n=1}^{N-1}\sum_{i=1,2}(t_n^{\parallel}a_{n,i}^{\dagger}a_{n+1,i} + \text{H.c.}) + \sum_{n=1}^{N}(t_n^{\perp}a_{n,1}^{\dagger}a_{n,2} + \text{H.c.}) \quad (3)$$

where $t_n^{\parallel}$ and $t_n^{\perp}$ are the nearest-neighbor hopping rates within and between the horizontal carbon atomic chains, respectively. Because of hydrogen passivation of the edge atoms, the carbon bonds at the edges are shorter by 3.3−3.5% compared to those in the middle of the ribbon, leading to a $\delta = 12\%$ increase in the corresponding hopping integrals.[46] In the present TB description, the effect of edge passivation can be well approximated by assuming $t_{1,N}^{\perp} = (1 + \delta)t$. Because of the Kekulé distortions, $t_n^{\parallel} = t_{n-1}^{\perp} = t$ for $n = 3p$, where $p = 1, 2, 3, \ldots$ is a positive integer, and $t_n^{\parallel} = t_n^{\perp} = t'$ for other values of n $(1 < n < N)$. The corresponding band structures can be obtained by diagonalizing H_r in the momentum space.

Similar to the cases of armchair GNRs, the band gaps of the armchair KGNRs as a function of the ribbon width are well separated into three different categories, given by $\Delta_{3p\pm1}$ and Δ_{3p} as illustrated in Figure 4b. In order to more clearly display the behaviors of band gap variations, we adopt λ-values that are enlarged from those obtained by fitting the band structures shown in Figure 3b,c. However, the intriguing qualitative features revealed should not rely explicitly on the magnitude of λ (see the last paragraph in the Supporting Information). In the present systems, Δ_{3p-1} undergoes a gap closing and reopening process upon increasing the ribbon width. This intriguing nonmonotonous scaling behavior is rooted in the delicate competitions of three different gap opening mechanisms: quantum confinement, edge passivation, and Kekulé distortions. In contrast, Δ_{3p+1} and Δ_{3p} still exhibit monotonous behaviors, approaching a common saturated value of the band gap given by $2|\lambda|$. Qualitatively, the quantum confinement effect can be characterized by $\Delta_N \sim W^{-1}$ with W as the ribbon width. To study the influence of the Kekulé distortions on the scaling behaviors of the band gaps, we also plot $\Delta_{3p\pm1}$ and Δ_{3p} as functions of both the ribbon width and strength of the Kekulé distortions. As shown in Figure 4c−e, Δ_{3p+1} and Δ_{3p} still increase monotonously with either decrease of the ribbon width or increase of the distortion strength, while Δ_{3p-1} displays distinctly nonmonotonous scaling behavior when $\lambda \neq 0$. Near the gap closing point, the electronic structures preserve linear dispersions, as shown in Figure 4f for the armchair KGNR system with $\lambda = -0.2$ eV and $N = 8$.

In order to make the competitions of different gap opening mechanisms more transparent, we next solve analytically the band gaps of the armchair KGNRs using a perturbation approach. We focus on the narrow width cases in which the Kekulé distortions are substantially weaker than the quantum size effects. The distortions can then be treated perturbatively, on equal footing as the edge passivation effect.[28] The scaling properties for the band gaps of the armchair KGNRs to the first orders of both δ and λ are given as (see Supporting Information for details)

DOI: 10.1021/acs.nanolett.6b05354
Nano Lett. XXXX, XXX, XXX−XXX

$$\Delta_{3p-1} = \Delta^0_{3p-1} + \left|\frac{2\delta t}{p} + \lambda\right|$$
$$\Delta_{3p} = \Delta^0_{3p} - \frac{\delta t}{3p+1} f_{e,1}(p) - \frac{\lambda}{3p+1} f_{k,1}(p)$$
$$\Delta_{3p+1} = \Delta^0_{3p+1} + \frac{\delta t}{3p+2} f_{e,2}(p) - \frac{\lambda}{3p+2} f_{k,2}(p) \quad (4)$$

where $\Delta^0_{3p-1} = 0$, $\Delta^0_{3p} = 2t\left[2\cos\left(\frac{p}{3p+1}\pi\right) - 1\right]$, and $\Delta^0_{3p+1} = 2t\left[1 - 2\cos\left(\frac{p+1}{3p+2}\pi\right)\right]$ are band gaps of armchair GNRs when $\delta, \lambda = 0$.[26−28] Here, $f_{e,k;1,2}(p)$ are defined as positive functions for any values of p. With $t = 2.7$ eV and $\delta = 0.12$, these first-order band gaps are in good agreement with the numerical results shown in Figure 4b−e. In particular, for $N = 3p - 1$, because $\lambda < 0$, the Kekulé distortions compete with the edge effect, leading to the nonmonotonous scaling behavior of Δ_{3p-1}. For $N = 3p$ and $3p + 1$, the Kekulé effects just give additional positive corrections to the band gaps.

In summary, we have systematically studied the electronic properties of a graphene monolayer or graphene nanoribbons proximity-coupled to topological insulators, revealing delicate competitions of different gap opening mechanisms. For a graphene monolayer, our first-principles studies have identified the Kekulé distortions instead of the prevailing belief of proximity-enhanced SOC effects to be responsible for opening a band gap in graphene. We have also developed a generic tight-binding description of the systems to exploit the competing gap opening mechanisms of such a Kekulé distorted graphene monolayer and graphene nanoribbons. For Kekulé distorted graphene, the band gap scales linearly with the strength of the distortions. In contrast, the band gaps of armchair KGNRs may display intriguing nonmonotonous dependence on the nanoribbon width, resulting from the delicate competitions of quantum confinement, edge passivation, and Kekulé distortions. These findings offer viable alternative approaches toward inducing tunable band gaps in graphene and graphene nanoribbons.

■ ASSOCIATED CONTENT

Supporting Information

The Supporting Information is available free of charge on the ACS Publications website at DOI: 10.1021/acs.nanolett.6b05354.

Detailed analytical derivations of the band gaps for armchair KGNRs. Scaling behaviors of the band gap for a realistic Kekulé distortion strength (PDF)

■ AUTHOR INFORMATION

Corresponding Author

*E-mail: zhangzy@ustc.edu.cn.

ORCID

Wei Qin: 0000-0003-1035-1130

Zhenyu Zhang: 0000-0001-5844-3558

Author Contributions

Z.N.L. and W.Q. contributed equally to this work.

Notes

The authors declare no competing financial interest.

■ ACKNOWLEDGMENTS

This work was supported by National Natural Science Foundation of China (Grants 11634011, 61434002, 11504357, and 11374273), and the National Key Basic Research Program of China (Grant 2014CB921103). The work was carried out at National Supercomputer Center in Tianjin, and the calculations were performed on TianHe-1(A).

■ REFERENCES

(1) Castro Neto, A. H.; Guinea, F.; Peres, N. M. R.; Novoselov, K. S.; Geim, A. K. *Rev. Mod. Phys.* **2009**, *81*, 109−162.
(2) Beenakker, C. W. J. *Rev. Mod. Phys.* **2008**, *80*, 1337−1354.
(3) Du, X.; Skachko, I.; Barker, A.; Andrei, E. Y. *Nat. Nanotechnol.* **2008**, *3*, 491−495.
(4) Kane, C. L.; Mele, E. J. *Phys. Rev. Lett.* **2005**, *95*, 226801.
(5) Xiao, D.; Yao, W.; Niu, Q. *Phys. Rev. Lett.* **2007**, *99*, 236809.
(6) Tworzydlo, J.; Snyman, I.; Akhmerov, A. R.; Beenakker, C. W. J. *Phys. Rev. B: Condens. Matter Mater. Phys.* **2007**, *76*, 035411.
(7) Schomerus, H. *Phys. Rev. B: Condens. Matter Mater. Phys.* **2010**, *82*, 165409.
(8) Qiao, Z.; Yang, S. A.; Feng, W.; Tse, W.-K.; Ding, J.; Yao, Y.; Wang, J.; Niu, Q. *Phys. Rev. B: Condens. Matter Mater. Phys.* **2010**, *82*, 161414.
(9) Qiao, Z.; Ren, W.; Chen, H.; Bellaiche, L.; Zhang, Z.; MacDonald, A. H.; Niu, Q. *Phys. Rev. Lett.* **2014**, *112*, 116404.
(10) Ren, Y.; Qiao, Z.; Niu, Q. *Rep. Prog. Phys.* **2016**, *79*, 066501.
(11) Weeks, C.; Hu, J.; Alicea, J.; Franz, M.; Wu, R. *Phys. Rev. X* **2011**, *1*, 021001.
(12) Ding, J.; Qiao, Z.; Feng, W. X.; Yao, Y. G.; Niu, Q. *Phys. Rev. B: Condens. Matter Mater. Phys.* **2011**, *84*, 195444.
(13) Jiang, H.; Qiao, Z.; Liu, H.; Shi, J.; Niu, Q. *Phys. Rev. Lett.* **2012**, *109*, 116803.
(14) Wang, Z.; Tang, C.; Sachs, R.; Barlas, Y.; Shi, J. *Phys. Rev. Lett.* **2015**, *114*, 016603.
(15) Giovannetti, G.; Khomyakov, P. A.; Brocks, G.; Kelly, P. J.; van den Brink, J. *Phys. Rev. B: Condens. Matter Mater. Phys.* **2007**, *76*, 073103.
(16) Zhou, S. Y.; et al. *Nat. Mater.* **2007**, *6*, 770−775.
(17) Gorbachev, R. V.; et al. *Science* **2014**, *346*, 448−451.
(18) Wang, E.; et al. *Nat. Phys.* **2016**, *12*, 1111−1115.
(19) Ren, Y.; Deng, X.; Qiao, Z.; Li, C.; Jung, J.; Zeng, C.; Zhang, Z.; Niu, Q. *Phys. Rev. B: Condens. Matter Mater. Phys.* **2015**, *91*, 245415.
(20) Hou, C.-Y.; Chamon, C.; Mudry, C. *Phys. Rev. Lett.* **2007**, *98*, 186809.
(21) Giovannetti, G.; Capone, M.; van den Brink, J.; Ortix, C. *Phys. Rev. B: Condens. Matter Mater. Phys.* **2015**, *91*, 121417.
(22) Gutiérrez, C.; et al. *Nat. Phys.* **2016**, *12*, 950−958.
(23) Fujita, M.; Wakabayashi, K.; Nakada, K.; Kusakabe, K. J. *J. Phys. Soc. Jpn.* **1996**, *65*, 1920−1923.
(24) Nakada, K.; Fujita, M.; Dresselhaus, G.; Dresselhaus, M. S. *Phys. Rev. B: Condens. Matter Mater. Phys.* **1996**, *54*, 17954−17961.
(25) Wakabayashi, K.; Fujita, M.; Ajiki, H.; Sigrist, M. *Phys. Rev. B: Condens. Matter Mater. Phys.* **1999**, *59*, 8271−8282.
(26) Ezawa, M. *Phys. Rev. B: Condens. Matter Mater. Phys.* **2006**, *73*, 045432.
(27) Brey, L.; Fertig, H. A. *Phys. Rev. B: Condens. Matter Mater. Phys.* **2006**, *73*, 235411.
(28) Son, Y.-W.; Cohen, M. L.; Louie, S. G. *Phys. Rev. Lett.* **2006**, *97*, 216803.
(29) Han, M. Y.; Özyilmaz, B.; Zhang, Y.; Kim, P. *Phys. Rev. Lett.* **2007**, *98*, 206805.
(30) Jin, K.-H.; Jhi, S.-H. *Phys. Rev. B: Condens. Matter Mater. Phys.* **2013**, *87*, 075442.
(31) Popov, I.; Mantega, M.; Narayan, A.; Sanvito, S. *Phys. Rev. B: Condens. Matter Mater. Phys.* **2014**, *90*, 035418.
(32) Lazzeri, M.; Attaccalite, C.; Wirtz, L.; Mauri, F. *Phys. Rev. B: Condens. Matter Mater. Phys.* **2008**, *78*, 081406.

DOI: 10.1021/acs.nanolett.6b05354
Nano Lett. XXXX, XXX, XXX−XXX

(33) Kresse, G.; Furthmüller, J. *Phys. Rev. B: Condens. Matter Mater. Phys.* **1996**, *54*, 11169−11186.
(34) Kresse, G.; Furthmüller, J. *Comput. Mater. Sci.* **1996**, *6*, 15−50.
(35) Perdew, J. P.; Burke, K.; Ernzerhof, M. *Phys. Rev. Lett.* **1996**, *77*, 3865−3868.
(36) Grimme, S.; Antony, J.; Ehrlich, S.; Krieg, H. *J. Chem. Phys.* **2010**, *132*, 154104.
(37) Methfessel, M.; Paxton, A. T. *Phys. Rev. B: Condens. Matter Mater. Phys.* **1989**, *40*, 3616−3621.
(38) Zhang, Y.; et al. *Nat. Phys.* **2010**, *6*, 584−588.
(39) Li, Y.-Y.; et al. *Adv. Mater.* **2010**, *22*, 4002−4007.
(40) Gao, L.; Guest, J. R.; Guisinger, N. P. *Nano Lett.* **2010**, *10*, 3512−3516.
(41) Sutter, P.; Cortes, R.; Lahiri, J.; Sutter, E. *Nano Lett.* **2012**, *12*, 4869−4874.
(42) Zhang, J.; Triola, C.; Rossi, E. *Phys. Rev. Lett.* **2014**, *112*, 096802.
(43) Reich, S.; Maultzsch, J.; Thomsen, C.; Ordejón, P. *Phys. Rev. B: Condens. Matter Mater. Phys.* **2002**, *66*, 035412.
(44) Son, Y.-W.; Cohen, M. L.; Louie, S. G. *Nature (London, U. K.)* **2006**, *444*, 347−349.
(45) Miyamoto, Y.; Nakada, K.; Fujita, M. *Phys. Rev. B: Condens. Matter Mater. Phys.* **1999**, *59*, 9858−9861.
(46) Porezag, D.; Frauenheim, Th.; Köhler, Th.; Seifert, G.; Kaschner, R. *Phys. Rev. B: Condens. Matter Mater. Phys.* **1995**, *51*, 12947−12957.
(47) Zhang, W.; Yu, R.; Zhang, H.-J.; Dai, X.; Fang, Z. *New J. Phys.* **2010**, *12*, 065013.

DOI: 10.1021/acs.nanolett.6b05354
Nano Lett. XXXX, XXX, XXX−XXX